Simulation of Hypervelocity Scramjet Combustion with Oxygen Enrichment

D. Petty [1], M. K. Smart [1], V. Wheatley [1] and S. A. Razzaqi [1]

[1] *Centre for Hypersonics, The University of Queensland, Brisbane, Queensland, 4072, Australia*

Summary: A numerical investigation of oxygen enriched combustion within a hypervelocity scramjet was performed using two-dimensional Reynolds-averaged Navier-Stokes simulations. The simulations modelled previous oxygen enrichment experiments in a simplified scramjet flow-path. It is shown that oxygen enrichment significantly affects the mixing and combustion characteristics within a scramjet combustor. Simulation results indicate that combustion efficiency of the scramjet improved beyond the amount expected from the O_2 premixed with the fuel reacting with the stoichiometric quantity of H_2.

Keywords: hypervelocity, scramjet, oxygen enrichment, air-breathing.

Introduction

Air-breathing propulsion systems, such as the scramjet engine, with access-to-space capability have attracted considerable interest due to the current dependency on multi-stage rockets with low specific impulse. A three-stage rocket-scramjet-rocket system has been proposed to power a launch vehicle into a low Earth orbit [1]. The launch vehicle will travel at near-constant dynamic pressure during the operation of the scramjet. Results from the study showed that such a vehicle would struggle to maintain net thrust above Mach 12. This restricts the usefulness of scramjet engines for space access.

The difficulty of scramjet engines maintaining net thrust at higher altitudes is contributed by both air (specifically O_2) mass capture and residence time of O_2 within the combustor decreasing. These effects can be illustrated by performing a simple analysis. Air density of the atmosphere decreases by three orders of magnitude when travelling from the Earth's surface to an altitude of 47km [2]. Species mass fractions remain effectively constant within these altitudes so the mass of O_2 per unit volume of air decreases linearly with air density. Dynamic pressure variations are minimal in order to generate sufficient lift whilst avoiding excessive drag and heating loads [3]. Using the definition of dynamic pressure (q) and the one-dimensional continuity equation, the mass flow capture ($\dot{m}_C$) of a scramjet engine can be defined as:

$$\dot{m}_C = 2\frac{q_\infty A_C}{v_\infty} \tag{1}$$

This relationship shows that for trajectories which traverse along near constant dynamic pressure paths, the mass flow capture of the engine is inversely related to the flight speed (v_∞). Variations in capture area (A_C) are trivial in comparison to the increase in flight speed as the vehicle accelerates so mass capture must decrease with increasing altitude. The adverse effect of diminishing O_2 mass capture on scramjet performance is further compounded by the decreasing residence time of flow within the scramjet engine as flight speeds increase. It can be concluded from these factors that achieving high combustion efficiency is paramount in

hypervelocity scramjet engines. It is critical that effective mixing of air and fuel at the molecular level to a near stoichiometric mixture of O_2 and fuel occurs [3].

Oxygen enrichment is a technique aimed at supplementing the diminishing amount of O_2 capture at altitudes and speeds where scramjet shutoff is predicted to occur. The addition of O_2 has two additional effects at any altitude: the injected flow shifts towards a stoichiometric mixture of fuel and oxidizer as well as changing the fluid properties of the injected flow [4]. Pike [5] showed for a restricted class of scramjets that the addition of O_2 to the injected fuel decreased launch mass of a vehicle whilst increasing the payload mass.

Shock tunnel experiments simulating hypervelocity conditions were conducted by Razzaqi & Smart [6] to investigate the effectiveness of oxygen enrichment within a simplified scramjet engine. Oxygen enrichment was found to be effective at increasing the thrust of the scramjet, particularly at high altitudes. However, as only pressure transducer point measurements were taken, the details of the flow physics that led to the improved performance were not presented.

This paper attempts to reveal the details of the flow physics by carrying out a numerical investigation of Razzaqi and Smart's experiments. This report is structured as follows: first we present an overview of the Razzaqi and Smart experiment [6], then the numerical methodology employed for this study is described and finally, the results obtained are presented, focusing on combustion efficiency comparisons.

Oxygen Enrichment Experiments

The Razzaqi & Smart experiments were performed in the T4 free piston reflected shock tunnel at The University of Queensland [7]. The experiment utilized a contoured axisymmetric nozzle to produce two effective flight altitude conditions: standard altitude with M_∞ = 12.3 and q_∞ = 40.2 kPa and high altitude with M_∞ = 11.4 and q_∞ = 9.8 kPa. The numerical simulations performed for this study focused specifically on the standard altitude conditions. Two high range PCB pressure transducers were mounted in the stagnation region to record the nozzle-supply pressure [6]. A summary of the selected experimental shock tunnel conditions for simulation is detailed in Table 1.

Table 1: Summary of selected shock tunnel test conditions

Shot	Inflow	Composition	Temp (K)	Pres. (kPa)	Mach No. (-/-)	Mass Flow (kg/sec)
9941	Nozzle Exit	Air	988	6.3	5.7	N/A
	Injector	Off	N/A	N/A	N/A	N/A
9952	Nozzle Exit	N_2	958	5.9	5.9	N/A
	Injector	H_2	300 (t)	300 (t)	~ 1	0.0193
9953	Nozzle Exit	Air	986	6.4	5.7	N/A
	Injector	H_2 (ϕ=0.84)	300 (t)	301 (t)	~ 1	0.0194
9944	Nozzle Exit	Air	950	6.11	5.7	N/A
	Injector	H_2 (ϕ=0.81) + Oxy (EP~15%)	300 (t)	471 (t)	~ 1	0.0183 + 0.0272

Sequentially, these shots correspond to air only (no fuel injection), mixing only (fuel injected into N_2), combustion, and combustion with oxygen enrichment. The fuelling conditions of both simulation and experiment are described using the standard definition of fuel equivalence ratio (ϕ) for hydrogen fuel:

$$\phi = \frac{1}{2}\frac{M_{O_2}}{M_{H_2}}\frac{\dot{m}_{H_2,IN}}{0.23\dot{m}_C} \tag{2}$$

Where M_{O_2} is the molar mass of O_2, M_{H_2} is the molar mass of H_2, $\dot{m}_{H_2,IN}$ is the mass flow rate of injected H_2, $\dot{m}_C$ is the mass flow rate of ingested O_2.

The oxygen enrichment shot employed an additional flow (Oxy) of 75/25 (% by wt) O_2/N_2 mixture which was premixed with the fuel flow before injection. The parameter used to describe the amount oxygen enrichment is equivalent to the Enrichment Percentage (*EP*) used by Razzaqi & Smart [6]. This parameter is defined as the percentage of injected H_2 which would be consumed in a stoichiometric reaction with the injected enrichment oxygen:

$$EP = 2\frac{M_{H_2}}{M_{O_2}}\frac{\dot{m}_{O_2,IN}}{\dot{m}_{H_2,IN}} \times 100\% \tag{3}$$

Where $\dot{m}_{O_2,IN}$ is the mass flow rate of injected O_2. The objective of this set of experiments was to investigate the effect of varying EP whilst holding $\dot{m}_{H_2,IN}$ and $\dot{m}_C$ relatively constant.

The experimental model consists of three primary features: a two-dimensional compression wedge at an angle of 8° to the flow, a constant area rectangular combustor (duct) that has an aspect ratio of l/h = 18.4 and an expansion surface inclined at an angle 11° to the flow direction

The duct has a height of 47 mm and a width of 100 mm. An injector strut with a height of 7 mm injects fuel through a 1 mm × 100 mm slot located on the backward face. A cross-sectional schematic of the experimental test section is shown in the Fig. 1.

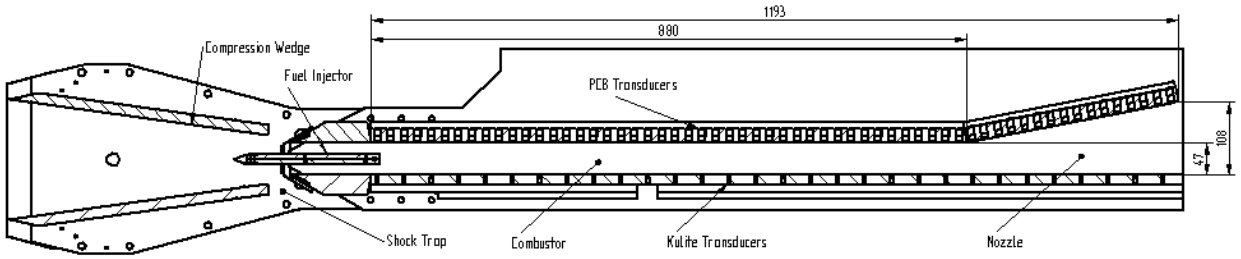

Fig. 1: Experimental model schematic [6]

The findings of the experimental campaign of [6] validated the previous theoretical findings, showing that specific thrust linearly increases with equivalence ratio at a particular oxygen enrichment percentage.

Determination of combustion efficiency from the experimental data required the use of a quasi one-dimensional cycle analysis method [8]. The analysis assumes a thermally perfect mixture of gases in thermal equilibrium. Skin friction drag and heat transfer across the duct walls were approximated using the Reynolds analogy. A combustion efficiency curve, taken from Heiser and Pratt [3], was used to model the effective mixing and kinetics of combustion

Employing this cycle analysis to predict pressure values along the duct, the combustion efficiency curve was manipulated to best match the experimental pressure measurements taken along the lower surface of the duct (Kulite transducers). Once pressure values were matched, the derived combustion efficiency curve was considered representative of the true combustion within the experimental duct, as shown in *Fig. 2*.

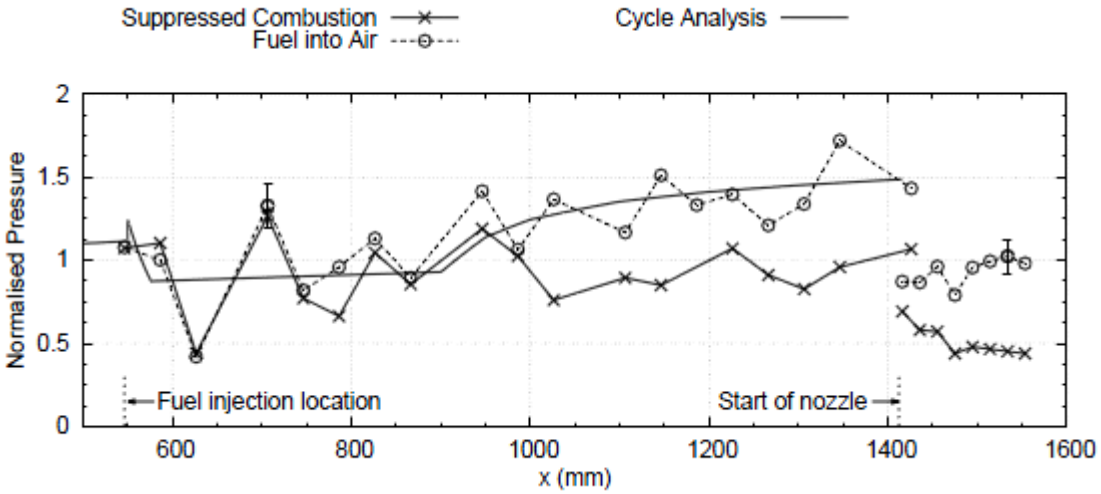

Fig. 2: Typical cycle predicted and experimental pressure distributions [8]

Using this method, the combustion efficiencies for shots 9953 and 9944 were found to be 45% and 60% respectively. It was concluded that combustion efficiency increased by an amount equivalent to the enrichment percentage.

Numerical Methodology

NASA's viscous upwind algorithm for complex flow analysis (VULCAN) version 6.1.0 [9] was the numerical solver used in this investigation. Vulcan can simulate two and three dimensional flows on multi-block structured grids by solving cell-centred integral forms of the Reynolds-averaged Navier-Stokes (RANS) equations [10].

The Diagonalized Approximate Factorization (DAF) temporal advancement scheme was used to achieve steady state solution convergence with a Courant-Friedrich-Lewy (CFL) regime ranging from 0.1 to 3.0.

The fluid is treated as a thermally prefect mixture of gas that obeys empirically derived 3-interval 9-coefficient caloric curve fits, for temperatures between 200 and 20,000 K.
The combustion of hydrogen was modelled using the 9 species and 18 finite rate reactions described and validated by Drummond [11].

Turbulence was modelled using Wilcox's k-ω model [12]. This model was shown to reliably simulate mixing layers by Cutler *et al.* [13]. A second order accurate scheme was used for the convective terms in the turbulence equations. Sutherland's law is used to compute the molecular viscosity. Thermal conductivity is computed from viscosity assuming constant Prandtl number. The molecular diffusion coefficient is computed from viscosity assuming constant Schmidt number.

Numerical modelling of the Razzaqi & Smart experiment is relatively straightforward due to the simple geometry of the experimental model. The two-dimensional grids were separated into two regions: the compression wedge and the combined rectangular combustor with expansion surface. The process was performed using Pointwise version 16.03R2 [14].

Uniform inflow conditions, equivalent to the respective shock tunnel exit conditions, were applied at the inflow boundary of the compression wedge region. The test section walls have been modelled using the isothermal (300K) law of the wall boundary conditions (BC) implemented in Vulcan (unless otherwise stated). Injected inflow conditions utilise the generic subsonic inflow BC implemented in VULCAN. First order extrapolated BCs were applied at the outflow boundaries.

Results

All simulations performed were based on the previously mentioned shock tunnel experiments (refer to Table 1) except the nominal 5% oxygen enrichment case. This simulation used the same injected flow conditions as the nominal 15% oxygen enrichment case but replaced the 75/25 (% by wt) O_2/N_2 mixture with air. A summary of the RANS simulations performed and the corresponding Razzaqi and Smart experiments is detailed in Table 2.

Table 2: Summary of RANS simulations of the Razzaqi & Smart experiment

Simulation	Shot	Cells	Turbulence Model	Wall Model	Chemistry Model
Fuel-off, 2D coarse grid	9941	200K	k-ω	Yes	No
Fuel-off, 2D fine grid	9941	686K	k-ω	Yes	No
Fuel-off, 2D fine grid without wall model	9941	686K	k-ω	No	No
3D compression wedge, coarse grid	9941	2.5M	k-ω	Yes	No
Mixing-only	9952	233K	k-ω	Yes	No
Fuel-on	9953	233K	k-ω	Yes	9×18 FR
5% Oxygen enrichment	N/A	233 K	k-ω	Yes	9×18 FR
15% Oxygen enrichment	9944	233 K	k-ω	Yes	9×18 FR

Duct Entrance Flow Conditions

The initial stage of each simulation required determining the flow through the compression wedge into the duct. The flow exiting this plane was used as the inflow conditions for the second grid region (which models the duct and expansion surface).

Compressible two-dimensional flow (oblique shock and Prandtl-Meyer expansion) relations were used to determine theoretical duct entrance conditions for each experimental shot for comparison. A summary of the computed duct entrance conditions is detailed in Table 3.

Table 3: Summary of computed duct entrance conditions

Shot	Method	Temp. (K)	Static Pres. (kPa)	Vel_x (m/sec)	$\dot{m}_C$ (kg/sec)
9941	Theoretical	1877	40.6	3200	0.791
9941	2D RANS	2060	40.8	3070	0.704
9952	Theoretical	1824	39.5	3160	0.782
9952	2D RANS	2000	39.9	3020	0.685
9953	Theoretical	1893	39.9	3330	0.781
9953	2D RANS	2130	42.0	3180	0.701
9944	Theoretical	1874	40.7	3200	0.792
9944	2D RANS	2060	40.8	3100	0.703

Injector Flow Conditions

Injector conditions were calculated using a quasi one-dimensional flow analysis assuming a thermally and calorically perfect gas with the following boundary conditions: a total temperature of 300 K, choked flow through the injector throat and a mass flow rate based on experimentally measured values (refer to Table 1).

Validation

Simulations using a fine grid without a wall function, a fine grid with a wall function and a medium grid with a wall function of the fuel-off case (Shot 9941) were performed to ensure grid convergence. Comparison of the results obtained using these computational grids, based upon pressure values along the duct centreline, showed acceptably minor variation, as shown in Fig. 3.

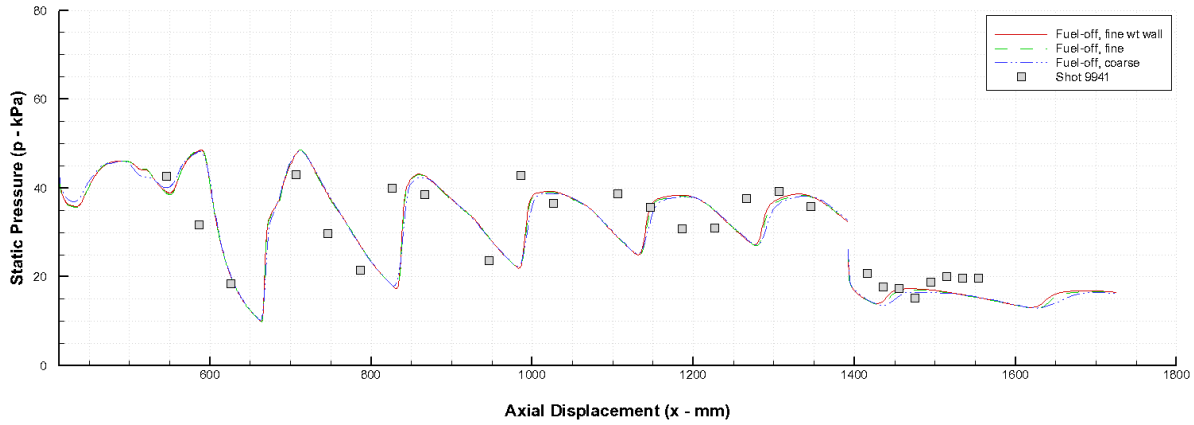

Fig. 3: Air Only CFD and experimental duct static pressure comparison

A comparison between the experimentally measured and simulated static pressures along the duct centreline was performed in order to validate the simulation, as shown in Fig. 3 for the air only case (Shot 9941) and Fig. 4 for the combustion cases (Shot 9953 & 9944). The magnitude of simulated and experimentally measured pressures is in close agreement. However, the difference between simulated and experimental shock reflection locations increases as the flow travels downstream towards the expansion surface. Three dimensional effects may be responsible for these discrepancies, as discussed in a later section.

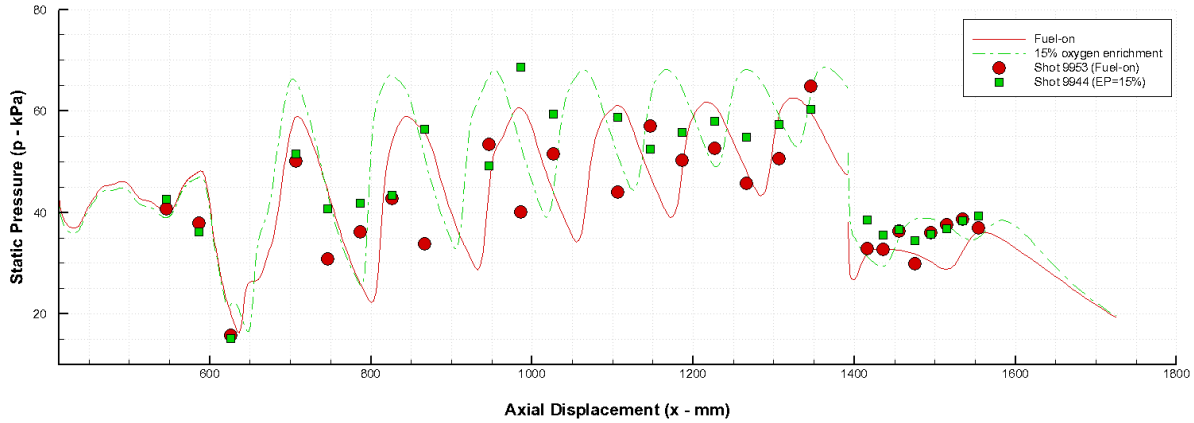

Fig. 4: Fuel into Air CFD and experimental duct static pressure comparison

The simulations predict the experimentally observed pressure rise along the duct for flows which experience combustion, as shown in Fig. 4. Positioning of the shock reflections is more difficult to discern from the experimentally measured pressures since fluctuations are not as clearly evident for the combustion cases.

Recirculation Region

A noteworthy feature of the mean flow through the duct is the recirculation region which forms behind the injection strut, shown in Fig. 5. This region contains low pressure recirculated flow which causes injected flow to be under-expanded just downstream from the point of injection. The injected flow expands until it meets the ingested flow travelling through the duct. In the fuel-on case, a Mach disk then forms in the injected flow causing it to become subsonic. In the nominal 15% oxygen enrichment case, the flow structure is altered: the injected flow is recompressed by a series of oblique shocks rather than by a Mach disk. The strength of the shear layer generated between the injected and ingested flows, which should induce strong mixing between the streams, varies significantly between the cases.

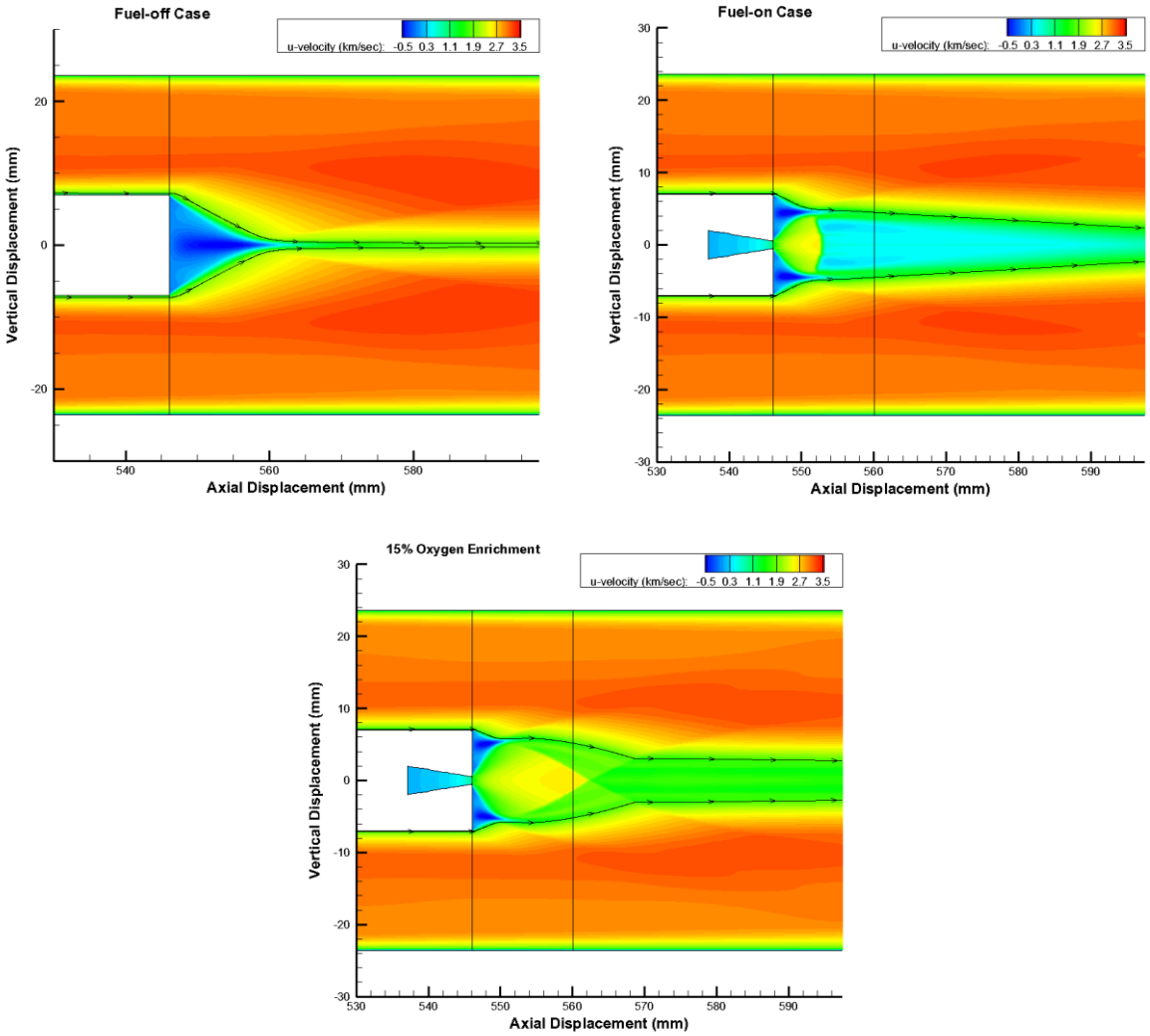

Fig. 5: Axial velocity contours behind the injector strut

Mixing and Combustion Characteristics

Ignition, identified by the net production of OH^- radicals, occurs approximately 40 mm downstream from the point of fuel injection (both for fuel only and oxygen enrichment cases) as can be seen in Fig. 6. The intensity of OH^- production is much higher in the oxygen enrichment case.

Completion of H_2 combustion, identified by the net production (formation) of H_2O, occurs within 1mm downstream of initial liberation of OH^- radicals (both for fuel only and oxygen enrichment cases), shown in Fig. 7. Further, a significantly stronger reaction region occurs at an axial displacement of 760 mm in the oxygen enrichment case.

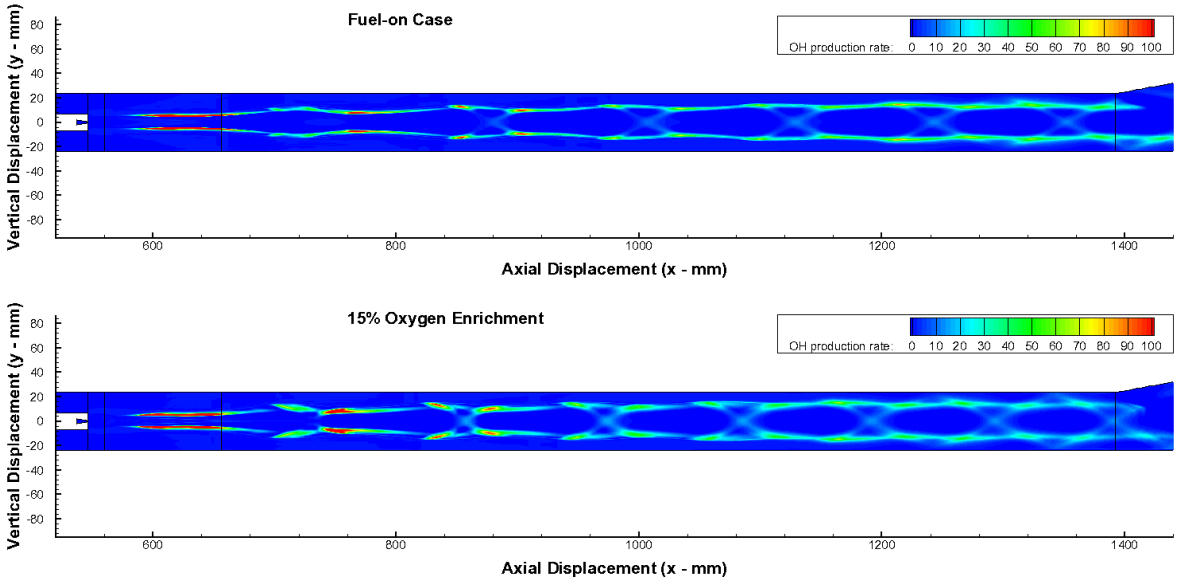

Fig. 6: OH production rate contours along the duct

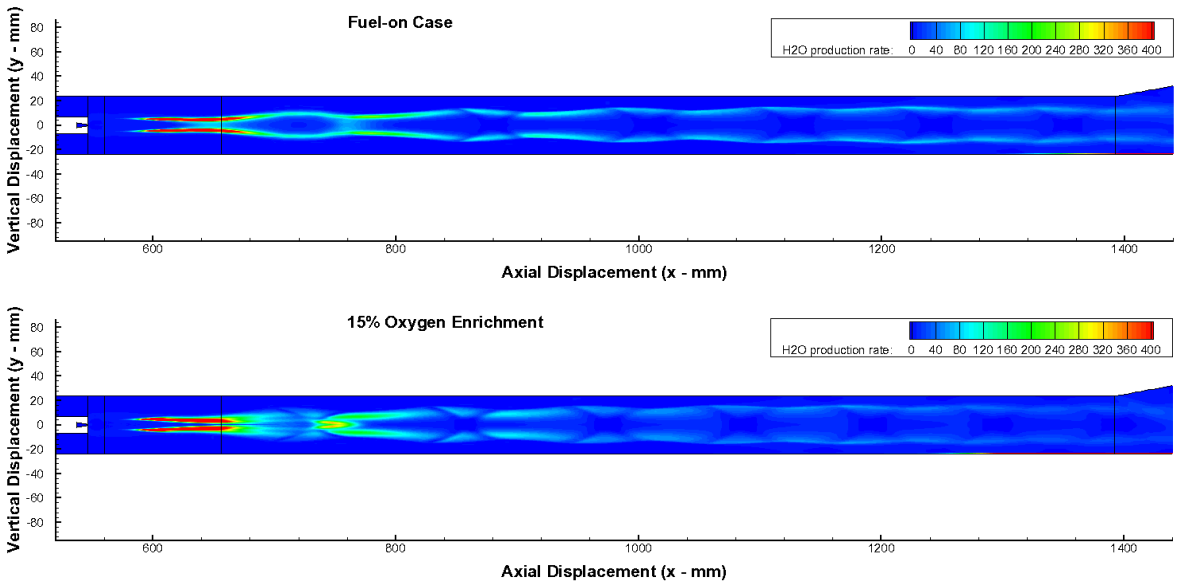

Fig. 7: H_2O production rate contours along the duct

The additional flow characteristics apparent in the oxygen enrichment case noticeably burn a greater amount of the injected H_2, shown in Fig. 8.

The combustion efficiency (η_C) of the combustor is give by the ratio of H_2O mass flow exiting the simulated combustor to the expected H_2O mass flow produced by completely combusting the injected H_2:

$$\eta_C = \frac{M_{H_2}}{M_{H_2O}} \frac{\dot{m}_{H_2O,EXIT}}{\dot{m}_{H_2,IN}} \tag{4}$$

Where M_{H_2O} is the molar mass of water and $\dot{m}_{H_2O,EXIT}$ is the mass flow of water exiting the duct.

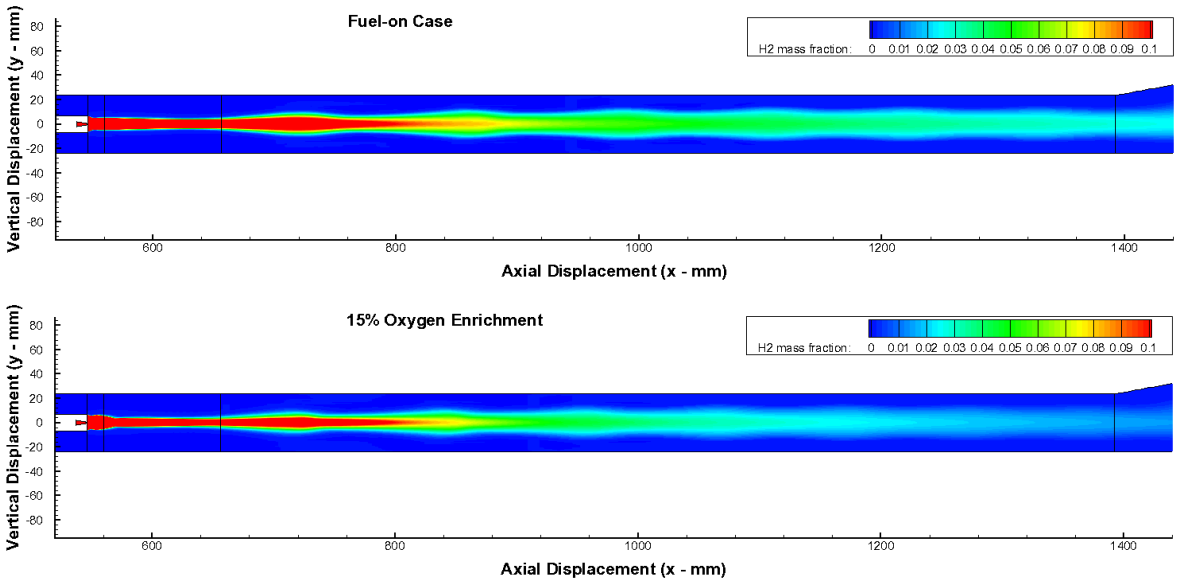

Fig. 8: H_2 mass fraction contours along the duct

For the fuel only case, combustion can only occur between the injected H_2 and the ingested O_2. However, oxygen enrichment cases provide a second source of O_2 which is premixed with the injected H_2. This allows the injected H_2 to combust with both the premixed O_2 and the ingested O_2. For this reason, in the case of oxygen enrichment, combustion efficiency is not a direct measure of the increased combustion strictly caused by the available H_2 combusting with the atmospheric O_2.

It is reasonable to expect the stoichiometric amount of H_2 premixed with the enrichment oxygen will combust completely due to the high combustor temperature. Subsequently, this amount of H_2 cannot react with the ingested atmospheric O_2 residing in the combustor. The efficiency with which the remaining H_2 (after premixed combustion) reacts with the atmospheric O_2 is defined as the compensated combustion efficiency ($\eta_{C,EPC}$):

$$\eta_{C,EPC} = \frac{100\% \times \eta_C - EP}{100\% - EP} \tag{5}$$

A summary of combustion parameters is detailed in Table 4.

Table 4: Summary of Combustion Parameters

Simulation	ϕ CFD	EP CFD (%)	Temp. (K)	η_C Experiment	η_C CFD	$\eta_{C,EPC}$ CFD
Fuel-on	0.84	N/A	2540	45	52.32	N/A
5% Oxygen enrichment	0.81	4.4	2610	N/A	57.98	56.04
15% Oxygen enrichment	0.81	14.1	2730	60	62.72	56.40

All three simulations have a similar equivalence ratio of almost unity. The simulation results show for a premixed fuel percentage of 4.4%, an additional 5.7% of the injected H_2 is burnt in comparison to the fuel only (no premixing) case. This implies that an additional 1.3% of the injected H_2 has reacted with the ingested O_2 due to the secondary effects of oxygen enrichment.

As previously mentioned, the premixed fuel combustion reduces the amount of injected H_2 available to mix and combust with the ingested O_2. The compensated combustion efficiency values show that both oxygen enrichment cases cause an additional 4% of the remaining available H_2 (after premixed combustion) to react with the ingested O_2.

Three-Dimensional Effects

One possible explanation for the mismatch of pressure distributions between simulated and experimental results could be the three-dimensional effects caused by the sidewalls of the experimental model. To investigate the uniformity of the flow entering the duct in the cross-stream direction, a three-dimensional simulation of the compression wedge was performed. Cross-flow velocities of up to 8% of the axial flow velocities were observed in the results of this simulation, shown in Fig. 9. This indicates that three dimensional effects may contribute significantly to the discrepancies between the numerical and experimental pressure distributions along the duct centreline. For example, changes in the axial Mach number within the duct will alter the location and strength of the shock pattern.

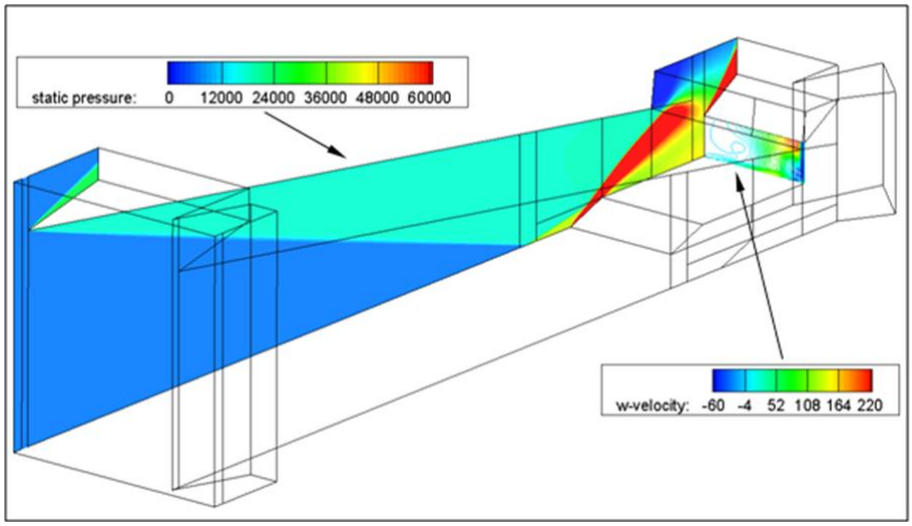

Fig. 9: Static pressure through the wedge and cross-flow velocity entering the duct

Conclusion

A numerical investigation using Reynolds-Averaged Navier-Stokes simulations was presented. This investigation provides new details on the flow physics within an oxygen enriched scramjet combustor. The simulation results show that oxygen enrichment affects the internal flow structure within the particular scramjet combustor. Specifically, oxygen enrichment affects the mixing and combustion characteristics within the combustor. The influence of oxygen enrichment on combustion is most significant in the ignition region. Improvements to combustion efficiency can be made beyond the percentage of premixed and injected O_2. For example, an enrichment percentage of 4.4% produces an increase in combustion efficiency of 5.7%.

References

1. Smart M.K. and Tetlow, M.R., "Orbital Delivery of Small Payloads using Hypersonic Airbreathing Propulsion", *Journal of Spacecraft and Rockets*, Vol. 46, No. 1, 2009, pp. 117-125

2. NASA "U.S. Standard Atmosphere 1976", NASA-TM-X-74335

3. Heiser W.H. and Pratt, D.T., *Hypersonic Airbreathing Propulsion*, AIAA Education Series, AIAA, Washington DC, 1994

4. Rudakov, A.S and Krjutchenko, V.V., "Additional Fuel Component Application for Hydrogen Scramjet Boosting", *SAE Aerospace Atlantic Conference and Exposition*, Dayton, OH, USA, April 1990

5. Pike, J., "The Choice of Propellants: A Similarity Analysis of Scramjet Second Stages", *Philosophical Transactions: Mathematical, Physical and Engineering Sciences*, Vol. 357, 1999, pp. 2357-2378

6. Razzaqi, S.A. and Smart, M.K. "Shock Tunnel Experiments on Oxygen Enrichment in a Hydrogen Fuelled Scramjet", *16th AIAA/DLR/DGLR International Space Planes and Hypersonic Systems and Technologies Conference*, AIAA 2009-7429, Bremen, Germany, Oct. 19-22, 2009

7. Stalker, R. J., Recent Developments with Piston Free Drivers, *17th International Symposium on Shock Waves and Shock Tubes*, 1990, pp 96-107

8. Razzaqi, S.A., private communication, Sep. 2010

9. White, J.A. and Morrison, J.H., "A Pseudo-Temporal Multi-Grid Relaxation Scheme for Solving the Parabolized Navier-Stokes Equations", AIAA Paper 99-3360, 14th AIAA Computational Fluid Dynamics Conference, Jun. 28 – Jul. 1, 1999.

10. NASA, Vulcan version 6.1.0 User Manual, 2009

11. Drummond, J.P., "Numerical Simulation of a Supersonic Chemically Reacting Mixing Layer", NASA TM 4055, 1988

12. Wilcox, D.C., *Turbulence Modeling for CFD*, 3rd edn, DCW Industries, La Cañada, 2006

13. Cutler, A. D., Diskin, G. S., Drummond, J. P., and White, J. A., "Supersonic Coaxial Jet Experiment for Computational Fluid Dynamics Code Validation" *AIAA Journal*, Vol. 44, No. 3, 2006, pp. 585-592.

14. Pointwise Inc., Pointwise version 16.03R2 User Manual, 2010